A Low Frequency Fiber Optic Vibration Sensor

Yung-Li Lin[1], Mao-Hsiung Chen[2], Wuu-Wen Lin[3]

[1]Institute of Electrical Engineering, National Sun Yat-Sen University, 70 Lien-hai Rd. Kaohsiung 804, Taiwan, Republic of China.
[2]Institute of Electrical Engineering, National Sun Yat-Sen University, 70 Lien-hai Rd. Kaohsiung 804, Taiwan, Republic of China.
[3]Department of Occupational Safty & Hygiene, Ta Jen University, 20 Weishin Road, Yanpu Shiang, Pingtung, Taiwan 907, Republic of China.
(D943010021@student.nsysu.edu.tw)

Abstract

The reflection wavelength from a fiber Bragg grating (FBG) is sensitive to the variation of the strain and temperature. Our sensor configuration is made of an interferometer and fiber Bragg gratings. The vibration induces a strain of the fiber Bragg grating, and it makes a phase difference between those two light beams in the interferometer. A demodulation circuit is needed to detect the phase difference caused by the vibration. In this paper, the aim is focused on the vibration measurement for some complicated structures. A fiber optic sensor is designed as a vibration monitor. Compare with a traditional accelerometer, the fiber optic sensor is more flexible for field applications. An all fiber system with good accuracy is for low frequency vibration measurement.

In this paper, two kinds of vibration sensor head are designed and studied, the first one is a bending loss sensor head and the other is an optic fiber Bragg grating sensor head. The results are narrated as follows: (1) The dynamic range of the bending loss sensor head is about 50 dB. (2) The dynamic range of the optic fiber Bragg grating sensor head is 38 dB with test frequency range between 100 ~ 400 Hz, the noise level is around 1.95 x 10^{-2} rad.

Keywords: Fiber Optical Sensors, Vibration Sensors, Interferometer, Fiber Bragg Grating

1. Introduction

Structural born vibration is the most concern issue in industry. Traditionally, the accelerometer is usually used as the major monitoring device for vibration. As the structure to be measured getting more and more complexity, there is a trend that the sensor must be more compact, tinier and more lighting. Because the traditional accelerometers are suffered from its loading effect, their accuracy of measurement is suspected and cannot match the modern measurement requirement. Hence, the study of fiber optic vibration sensor becomes an urgent issue in this era. Because of the optic fiber sensor has high sensitivity, wide dynamic range, EMI immunity, low cost, electrically passive sensor, multiplex ability, and high reliability [1], they have already been applied to many physics field sensing, for example: vibration [2], sound, temperature, electric current [3, 4], pressure, etc...

Early telecommunication relied primarily on the use of coaxial cables. However, limited by bandwidth and transmission loss, coaxial cable could no longer satisfy the needs of modern telecommunication. Experiment report of optic fiber sensor did not come to available until as late as 1973. In recent years materials have been improving and the manufacturing techniques of optic fiber related optic components have been refining; technologies of research and production of optic fiber sensors are becoming matured with more pervasive application.

In 1987 Miers el at [5] proposed the use of microbend technology based sensors in vibration measurement of structure. They measured the force required for accelerating a mass with microbend displacement sensor. When a inertia mass is placed on a foundation and an accelerating force is applied onto the foundation, a relative acceleration existing between the foundation and such inertia mass cause microbend in optic fiber, and ultimately leads to the change in transduction power in optic fiber. Sensitivity of accelerometer and dynamic range are totally dependent on the rigidity of the beam of the foundation and the inertia mass affixed on it; its frequency response is approximately 1 kHz.

Gaussignac (1992) [6] el al. applied the optic fiber technology in composite structure. These are all the attention catching focus points, and the optic fiber features of light weight, fine radius, and anti-corrosion are fully exploited and used in the monitoring of internal structure of test objects. Now it is a new weapon for disaster monitoring.

Berkoff (1996) [7] reported a fiber Bragg grating transducer for the measurement of acceleration. Results obtained using interferometric wavelength-shift detection demonstrates a demodulated signal output range of 50-g rms with a minimum detectable signal of ~ 1 mg／$\sqrt{Hz}$.

Freal (1998) [8] developed a highly sensitive microbend horizontal fiber-optic accelerometer. This particular model is aimed at deployment in seismological research where minute accelerations must be detected. The device uses a cantilever beam and the compliance of an optical fiber mounted between deforming teeth to act as the springs in the accelerometer's spring-mass system. Acceleration is detected by sensing the movement of the mass relative to the case through the changes in the intensity of light propagating through the deformed fiber. Accelerations as small as 5 pg at 1 Hz have been detected with a dynamic range in excess of 90 dB.

Zhu (2003) [9] brought up a cantilever beam and fiber Bragg grating to measure acceleration. The cantilever induces strain on the grating, resulting in a Bragg wavelength change that is subsequently detected.

Gunselmann (2004) [10] reported a sensorless soft-landing control strategy for electromagnetical spring-mass actuators can offer high robustness and low energy consumption simultaneously. System was applied to various linear and rotational actuators in automotive applications such as the impulse charging, but it is suitable for all electromagnetical spring-mass actuators. High robustness was proven on fired engines under real application conditions.

Hence, a low cost vibration sensor in low frequency band is required.

2. Fiber Optic Sensor Design

In this paper, two kinds of vibration sensor head are designed, (1) bending loss sensor head: based on optic fiber micro-bending mechanism, to detect the loss of optic fiber bending due to physic field, (2) optic fiber Bragg grating vibration sensor head; physic field vibration induces a strain of the fiber Bragg grating mount on a cantilever beam.

2.1 Bending Loss Vibration Sensor

The design principle of this sensor is based on optical fiber micro-bending mechanism. Fig.1. shows the configuration of this sensor. In this sensor head, there is a base with wave like form on one side with a similar counterpart on its top. Several turns of optical fiber are wound around the base. The number of optic fiber turns increases the sensibility of the bending loss sensor.

Measurement values of vibration were determined by output intensity: I_o and input intensity: I_i. The curvatures of base must be greater than R_0, where R_0 is the minimum radius of optic fiber when bending loss could be ignored. R_0 is determined by twining 30 turns on the circumference of cylinders with different radius (5 ~ 50 mm), to measure the loss of transmit intensity by a power meter. The results shows that $R_0 \approx$ 30 mm。

This bending loss fiber optic vibration sensor is constructed of two pieces: 1. a simple pendulum; 2. a spring, namely a spring - mass system.

The diagram of the bending loss fiber optic vibration sensor is shown as Fig.1. To protect the optical fiber from being broken during vibration, we make the tooth like arc in round shape. In order to avoid moist and rust, base and mass buck are made of stainless.

2.2 FBG Vibration Sensor

The design of FBG vibration sensor, configuration of mechanism is a cantilever beam to bear a mass. The mechanism of the sensor is act as the springs in the accelerometer's spring-mass system. When determined the stiffness of spring and weight of mass then anticipated of monitoring frequency range will be obtained. The mechanism design of sensor is simply and easy to maintain. The FBG vibration sensor purpose to design is for monitoring low frequency range.

In order to prevent the FBG from rupturing under strong vibration, FBG with Teflon protection before use and sealed up by Epoxy, then put it on mechanism.

The governing equation of the spring-mass system is listed as below:

$$EI\frac{\partial^4 v}{\partial x^4} + m\frac{\partial^2 v}{\partial t^2} = 0 \tag{1}$$

where $v\ (x,\ t)$ is the modal function, m and EI are the mass and the flexural strength of the cantilever beam, respectively. Its boundary conditions are:

$$\begin{cases} v(0,\ t) = 0, & \dfrac{\partial v}{\partial x}\Big|_{x=0} = 0 \\ \dfrac{\partial^2 v}{\partial x^2}\Big|_{x=0} = 0, & \dfrac{\partial^2 v}{\partial x^2}\Big|_{x=l} = 0 \end{cases} \tag{2}$$

The first three natural frequencies of the cantilever beam, derived by applying separation of variables and numeric method in equation (3), are: $\omega_1 = 3.52\ \omega_0$，$\omega_2 = 22.04\ \omega_0$，$\omega_3 = 61.70\ \omega_0$, where $\omega_0 = \sqrt{EI/ml^4}$; l: length of cantilever beam. Substituting the design values in, the corresponding sensor head third vibration mode resonance frequency are 40 Hz, 250 Hz and 700 Hz. The ones that show this paper design in the FBG vibration sensor head, fetch its frequency and respond more straight part, can invite quantity is examined to 40 Hz.

3. Optic Fiber Interferometer Design

The configuration of the fiber optic sensing system is shown in Fig. 4. The system is a Mach-Zenhder and Sagnac hybrid interferometer type. Because the Mach-Zehnder interferometer has the single sensing arm is easy to install, and Sagnac interferometer has the feature of zero optical path. Suitable for long distance is to install array sensor. Owing to the two light beam pass through and back the coupler twice, so that optical intensity compare with the other interferometer, the signal become weak. In order to overcome the problem, we can use an EDFA to amplify the optic signal [11].

The main system can be divided into 3 units as the following: (1) Light source units; It consists of a wide bandwidth ASE (Amplified Spontaneous Emission) light source and an optical isolator; (2) Sensing units; It includes several FBG's and a hybrid Mach-Zehnder and Sagnac interferometer; (3) Signal processing units; It includes a photodetector, and some follow up electronic signal processors.

In order to verify whether the mathematic analysis and concept of the design are correct, we used the Jones matrix to analyze the optical circuit. The block diagram of the Jones matrix is shown in Fig. 5.
The system is a Mach-Zenhder and Sagnac hybrid interferometer. The verification of it will be explained below:

3.1 Optical path diagram

According to the optical path diagram, the first optical path is from light source to the optical isolator, the first coupler 13, fiber 35, the second coupler 59, coupler loop, the second coupler 68, fiber 811, FBG reflected、fiber 118, the second coupler 87, fiber 74, the first coupler 42, finally to the detector.

The second optical path is from the source to the optical isolator, the first coupler 14, fiber 47, the second coupler 79, coupler loop, the second coupler 68, fiber 811, FBG reflected, fiber 118, the second coupler 85, fiber 53, the first coupler 32, finally to the detector.

The third optical path is from light source to the optical isolator, the first coupler 13, fiber 35, the second coupler 59, coupler loop, the second coupler 610, fiber 1013, from the FBG reflected、fiber 1310, the second coupler 107, fiber 74, the first coupler 42, finally to the detector.

The fourth optical path is from the source to the optical isolator, the first coupler 14, fiber 47, the second coupler 79, coupler loop, the second coupler 610, fiber 1013, FBG reflected, fiber 1310, the second coupler 105, fiber 53, the first coupler 32, finally to the detector.

The path 1: 1 → 3 → 5 → 9 → 6 → 8 → 11 → 12 → 11 → 8 → 7 → 4 → 2, path 2: 1 → 4 → 7 → 9 → 6 → 8 → 11 → 12 → 11 → 8 → 5 → 3 → 2, path 3: 1 → 3 → 5 → 9 → 6 → 10 → 13 → 14 → 13 → 10 → 7→ 4 → 2, and path 4: 1 → 4 → 7 → 9 → 6 → 10 → 13 → 14 → 13 → 10 → 5→ 3 → 2. From the analysis of these four optical paths, we find out though the four optical paths are different, but the lengths of these four optical paths are equal. Therefore, when the sensor system was induced by the vibration signal, the four optical paths always have a constant phase difference. Hence, this interferometer is a hybrid one with M-Z and Sagnac type.

3.2 The Jones matrix:

According to the optical path, we can draw the block diagram of the Jones matrix [12] as shown in Fig. 5. In order to calculate the interferometric effect of these optical paths, these optical components are substituted by their correspondent Jones matrices.

$E_o=[R]\ [K_{42}]\ [J_{74}]\ [K_{87}]\ [J_{118}]\ [F]\ [J_{811}]\ [K_{68}]\ [k\ loop]\ [K_{59}]\ [J_{35}]\ [K_{13}]\ E_i+[R]\ [K_{32}]\ [J_{53}]\ [K_{85}]\ [J_{118}]\ [F]\ [J_{811}]\ [K_{68}]\ [k\ loop]\ [K_{79}]\ [J_{47}]\ [K_{14}]\ E_i+[R]\ [K_{42}]\ [J_{74}]\ [K_{107}]\ [J_{1310}]\ [F]\ [J_{1013}]\ [K_{610}]\ [k\ loop]\ [K_{59}]\ [J_{35}]\ [K_{13}]\ E_i+[R]\ [K_{32}]\ [J_{53}]\ [K_{105}]\ [J_{1310}]\ [F]\ [J_{1013}]\ [K_{610}]\ [k\ loop]\ [K_{79}]\ [J_{47}]\ [K_{14}]\ E_i$

$$
\begin{aligned}
E_o =& \begin{bmatrix} -1 & 0 \\ 0 & 1 \end{bmatrix} \cdot a^{1/2} \begin{bmatrix} k_t & k_c \\ k_c & k_t \end{bmatrix} \cdot \begin{bmatrix} e^{-j\phi} & 0 \\ 0 & 1 \end{bmatrix} \cdot \exp(j\phi_1) \cdot \frac{1}{\sqrt{3}} \exp j(\phi_{87}) [I] \cdot \begin{bmatrix} e^{-j\phi} & 0 \\ 0 & 1 \end{bmatrix} \cdot t_T \begin{bmatrix} a & b \\ b^* & a \end{bmatrix} \cdot \exp(j\phi_{v1}) \cdot \begin{bmatrix} e^{j\phi} & 0 \\ 0 & 1 \end{bmatrix} \cdot \\
& \frac{1}{\sqrt{3}} \exp(j\phi_{68}) [I] \cdot \frac{1}{\sqrt{3}} \exp(j\phi_{96}) [I] \cdot \frac{1}{\sqrt{3}} \exp(j\phi_{59}) \cdot [I] \cdot \begin{bmatrix} e^{j\phi} & 0 \\ 0 & 1 \end{bmatrix} \cdot a^{1/2} \begin{bmatrix} k_t & k_c \\ k_c & k_t \end{bmatrix} \cdot E_i + \begin{bmatrix} -1 & 0 \\ 0 & 1 \end{bmatrix} \cdot a^{1/2} \begin{bmatrix} k_t & k_c \\ k_c & k_t \end{bmatrix} \cdot \\
& \begin{bmatrix} e^{-j\phi} & 0 \\ 0 & 1 \end{bmatrix} \cdot \frac{1}{\sqrt{3}} \exp(j\phi_{85}) \cdot [I] \cdot \begin{bmatrix} e^{-j\phi} & 0 \\ 0 & 1 \end{bmatrix} \cdot t_T \begin{bmatrix} a & b \\ b^* & a \end{bmatrix} \cdot \exp(j\phi_{v2}) \begin{bmatrix} e^{j\phi} & 0 \\ 0 & 1 \end{bmatrix} \cdot \frac{1}{\sqrt{3}} \exp(j\phi_{68}) [I] \cdot \frac{1}{\sqrt{3}} \exp(j\phi_{96}) [I] \cdot \\
& \frac{1}{\sqrt{3}} \exp(j\phi_{79}) [I] \cdot \begin{bmatrix} e^{j\phi} & 0 \\ 0 & 1 \end{bmatrix} \cdot \exp(j\phi_2) \cdot a^{1/2} \begin{bmatrix} k_t & k_c \\ k_c & k_t \end{bmatrix} E_i + \begin{bmatrix} -1 & 0 \\ 0 & 1 \end{bmatrix} \cdot a^{1/2} \begin{bmatrix} k_t & k_c \\ k_c & k_t \end{bmatrix} \cdot \begin{bmatrix} e^{-j\phi} & 0 \\ 0 & 1 \end{bmatrix} \cdot \exp(j\phi_3) \cdot \\
& \frac{1}{\sqrt{3}} \exp(j\phi_{107}) [I] \cdot \begin{bmatrix} e^{-j\phi} & 0 \\ 0 & 1 \end{bmatrix} \cdot t_T \begin{bmatrix} a & b \\ b^* & a \end{bmatrix} \exp(j\phi_{v3}) \cdot \begin{bmatrix} e^{j\phi} & 0 \\ 0 & 1 \end{bmatrix} \cdot \frac{1}{\sqrt{3}} \exp(j\phi_{610}) [I] \cdot \frac{1}{\sqrt{3}} \exp(j\phi_{96}) [I] \cdot \\
& \frac{1}{\sqrt{3}} \exp(j\phi_{96}) [I] \cdot \frac{1}{\sqrt{3}} \exp(j\phi_{59}) [I] \cdot \begin{bmatrix} e^{j\phi} & 0 \\ 0 & 1 \end{bmatrix} \cdot a^{1/2} \begin{bmatrix} k_t & k_c \\ k_c & k_t \end{bmatrix} E_i + \begin{bmatrix} -1 & 0 \\ 0 & 1 \end{bmatrix} \cdot a^{1/2} \cdot \begin{bmatrix} k_t & k_c \\ k_c & k_t \end{bmatrix} \cdot \begin{bmatrix} e^{-j\phi} & 0 \\ 0 & 1 \end{bmatrix} \cdot \\
& \frac{1}{\sqrt{3}} \exp(j\phi_{105}) [I] \cdot \begin{bmatrix} e^{-j\phi} & 0 \\ 0 & 1 \end{bmatrix} \cdot t_T \begin{bmatrix} a & b \\ b^* & a \end{bmatrix} \exp(j\phi_{v4}) \cdot \begin{bmatrix} e^{j\phi} & 0 \\ 0 & 1 \end{bmatrix} \cdot \frac{1}{\sqrt{3}} \exp(j\phi_{610}) [I] \cdot \frac{1}{\sqrt{3}} \exp(j\phi_{96}) [I] \cdot \\
& \frac{1}{\sqrt{3}} \exp(j\phi_{79}) \cdot [I] \cdot \begin{bmatrix} e^{j\phi} & 0 \\ 0 & 1 \end{bmatrix} \cdot \exp(j\phi_4) \cdot a^{1/2} \begin{bmatrix} k_t & k_c \\ k_c & k_t \end{bmatrix} E_i \\
=& \frac{1}{9} t_T \begin{bmatrix} 0 & -j \\ j & 0 \end{bmatrix} \cdot \left\{ \cos \frac{\phi_1 + \phi_{v1} - \phi_2 - \phi_{v2} + 120^0}{2} \cdot e^{j(\frac{\phi_1+\phi_{v1}+\phi_2+\phi_{v2}}{2})} + \cos \frac{\phi_3 + \phi_{v3} - \phi_4 - \phi_{v4} + 120^0}{2} \cdot e^{j(\frac{\phi_3+\phi_{v3}+\phi_4+\phi_{v4}}{2})} \right\} \cdot E_i
\end{aligned}
\tag{3}
$$

Here, the Jones matrix of the fiber can be expressed as

$$\vec{J} = \frac{\alpha_s}{d_s} \begin{bmatrix} a_s & -b_s^* \\ b_s & a_s^* \end{bmatrix} = \begin{bmatrix} e^{j\phi} & 0 \\ 0 & 1 \end{bmatrix}$$

The Jones matrix of the FBG can be denoted as

$$\vec{F} = t_T \begin{bmatrix} a & b \\ b^* & a \end{bmatrix} \cdot \exp(j\phi_i) = t_T \begin{bmatrix} 1 & 0 \\ 0 & 1 \end{bmatrix} \cdot \exp(j\phi_i)$$

The Jones matrix of the coupler can be denoted as

$$\vec{K} = K_{ij} exp\left(j\phi_{ij}\right)[I]$$

where $exp(j\phi_{vi})$: the optical path difference of the measurand ($i=1, 2$)

The optical intensity is

$$I = \frac{1}{162} t_T^2 \begin{bmatrix} 1 & 0 \\ 0 & 1 \end{bmatrix} \cdot \left\{ 2 + \cos(\phi_1 + \phi_{v1} - \phi_2 - \phi_{v2} + 120^0) + \cos(\phi_3 + \phi_{v3} - \phi_4 - \phi_{v4} + 120^0) \right\} \cdot |E_i|^2 \tag{4}$$

Among them, the interference term can be expressed as:

Path 1 and path 2: $\frac{1}{162}\left\{\cos(\phi_1 + \phi_{v1} - \phi_2 - \phi_{v2} + 120^0)\right\}$ (5)

Path 3 and path 4: $\frac{1}{162}\left\{\cos(\phi_3 + \phi_{v3} - \phi_4 - \phi_{v4} + 120^0)\right\}$ (6)

4. Experimental Results and Discussion

4.1 Bending Loss Vibration Sensor

The experiment of the optic fiber bending loss vibration sensor, set it into dynamic vibrating loading test. The configuration of this test is shown in Fig. 2. The experiment procedures are list below. (1) To calibrate the Digital Optical Power Meter (Newport 1830-C) on shaking table, with one end of FC / APC pigtail connect to the light source on the power meter, the other end connected to the photodetector. Record the noise floor of the optical power meter. (2) Wound 3 turns optic fiber on base and spliced with FC / APC pigtail of one end. Set up the sensor deck on a shaking table, connected to light source, the other bare optic fiber end clamping by a photo detector device, and then connected it to the input on the power meter. (3) Put 100 g weight on the top (glue tight with adhesive tape). (4) The input status of the shaking table: 10、20、30、40、50 Hz sine-wave; the amplitude of vibration：0.2 ~ 1.0 ~ 0.2 g (m / s^2) each cycle; within a constant increasing of 0.2 g. (5) Recording the maximum level on display panel of the power meter.

The experimental record of maximum bending loss on shaking table status is shown in Fig. 3. The results show that there has the highest sensitivity: 41.21 dB in 10 Hz; when 1 g shaking table input condition.

4.2 FBG Vibration Sensor

The purpose of experiment is to verify that the FBG vibration sensor head is work. The system is used of a hybrid Mach-Zehnder and Sagnac type interferometer. The vibration induced by the free fall block impact the ground was measured. Then, the performance of the system in the low frequency range was monitored.

Fig. 5. is the diagram of the fiber optic sensing system. The FBG vibration sensor head is first put it in an aluminum box, then glue tightly with bonding adhesive and set up beside the road. Let the block was free falled from a 50 cm height above ground.

The signal detected by a spectrum is shown in Fig. 6. The result shows that there is an obvious higher level relative to the background noise within frequency range between 60 ~ 300 Hz. Dynamic range measured is about 30 dB in this testing. It denotes that the shows interferometric fiber optic vibration sensor we proposed is work. There is good response in the low frequency range, as we expected.

5. Conclusion

The fiber grating vibration sensor designed in this paper has the features of simple mechanical structure. It can be used in the measurement of estimated frequency range distributed in lower frequency range after set up. According to test result, it is proved that its response is suitable for use in low frequency range and maintenance cost is low for future applications. The shortage is that it is limited by the constraint of dead weight effect from the structure material of the mechanical structure itself. To gain higher system response sensitivity, heavier mass blocks should be selected for mechanical structure design to limit the response frequency range in the low frequency range.

In this paper, two kinds of vibration sensor head are designed and studied, the first is a bending loss sensor head and the other is an optic fiber Bragg grating sensor head. The results are narrated as follows: (1) The dynamic range of the bending loss sensing head is about 50 dB. (2) The dynamic range of the optic fiber Bragg grating sensing head is 38 dB with test frequency range between 100 ~ 400 Hz, the noise level is around 1.95×10^{-2} rad.

6. Acknowledgement

The authors would like to thank the research financial support from Ministry of Education, Taiwan.

Reference

[1]. K. K. Clay, D. Anthony, “Overview of High Performance Fiber-Optic sensing,” *Journal of Physics D: Applied Physics*, *2004 IOP Publishing Ltd Printed in the UK*, pp.R197-R216, 2004.

[2]. H. Lin, W. W. Lin, M. H. Cheng and S. C. Huang, “A Vibration Insensitive Reciprocal Reflection Interferometer for Optical Fiber Current Sensor,” *Opt. Eng.*, Vol.38, No.10, pp.1722-1799, Oct. 1999.

[3]. D. Kersey, “A Review of Recent Developments in Fiber Optic Sensor Technology,” *Optical Fiber Technology*, Vol. 2, pp.291-317, 1996.

[4]. Y. L. Lin, M. H. Chen and W. W. Lin, “The Feasibility Analysis of Monitoring Falling Stones by Means of a Fiber Optic Interferometer,” *SPIE-Int. Soc. Opt. Eng.*, Vol. 6174, 2006 (to be published).

[5]. D. R. Miers. et. al., “Design & Characterization of Fiber Optic Accelerometers,” *Proc. SPIE.* 838, E-E / Fibers, 87, San Diego, Calif., 1987.

[6]. J. M. Caussignac, A. Chabert, G. Morel, P. Rogez and J. Seantier, “Bearing of a Bridge Fitted with Load Measuring Devices Based on Optical Fiber Technology,” *Proc. SPIE-Int. Soc. Opt. Eng.* 1777, pp.207-210, 1992.

[7]. T. A. Berkoff and A. D. Kersey, “Experimental demonstration of a fiber Bragg grating accelerometer,” *IEEE Photonics Technology Letters*, Vol. 8, pp. 1677-1679, 1996.

[8]. J. Freal, C. Zarobila and C. Davis, “A microbend horizontal accelerometer for borehole deployment”, *J. Lightwave Technology*, Vol. 5, Issue 7, pp. 993-996, 1987.

[9]. Y. N. Zhu, P. Shum, C. Lu, B. M. Lacquet, P. L. Swart and S. J. Spammer, “Temperature-insensitive fiber Bragg grating,” *IEEE Photonics Technology Letters*, Vol. 15, pp. 1437-1439, 2003.

[10]. C. Gunselmann and J. Melbert, “Soft-landing control for sensorless electromagnetical spring-mass actuators,” *Proc.PEMD Conf. Publ.* No. 498 Vol. 2, pp.715-718, 2004.

[11]. W.W.Lin, S.C. Huang, J.S. Tsay and S.C. Hung," System Design and Experimental Investigation of Optically Amplified Time-Division-Multiplexing of Polarization -Insensitive Fiber Optic Michelson Interferometric Sensor,” J. Lightwave Technol., Vol.18, No.3, pp.348~359., Mar. 2000. (SCI)

[12]. W. W. Lin, “The Configuration Analysis of Fiber Optic Interferometers for Hydrophones,” 2004 OCEANS ’04 MTS / IEEE Conference, Chuo-ku, Kobe, Japan, pp.589-592, Nov. 09-12, 2004.

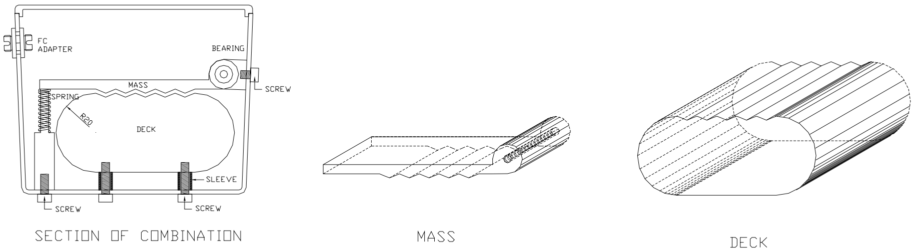

Fig.1.   Bending loss vibration sensor head

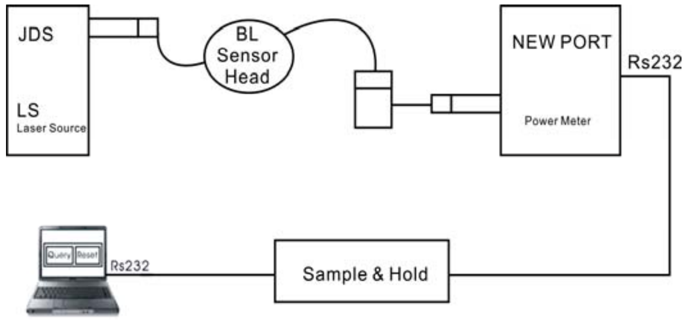

Fig.2. The experiment configuration of bending loss sensing system

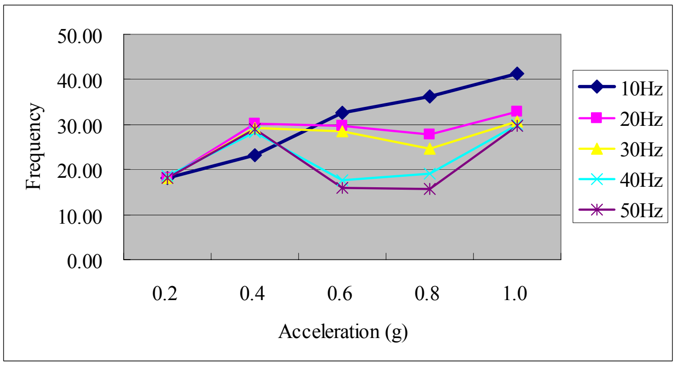

Fig.3. The experiment result of bending loss sensing system

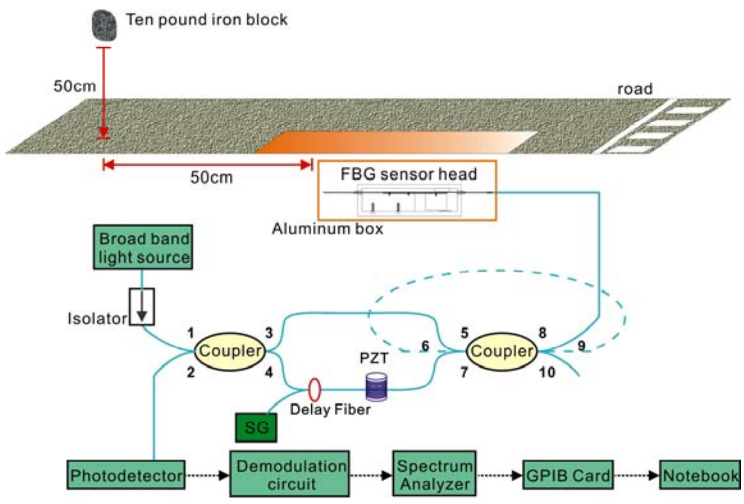

Fig.4. The experiment configuration of vibration sensing system

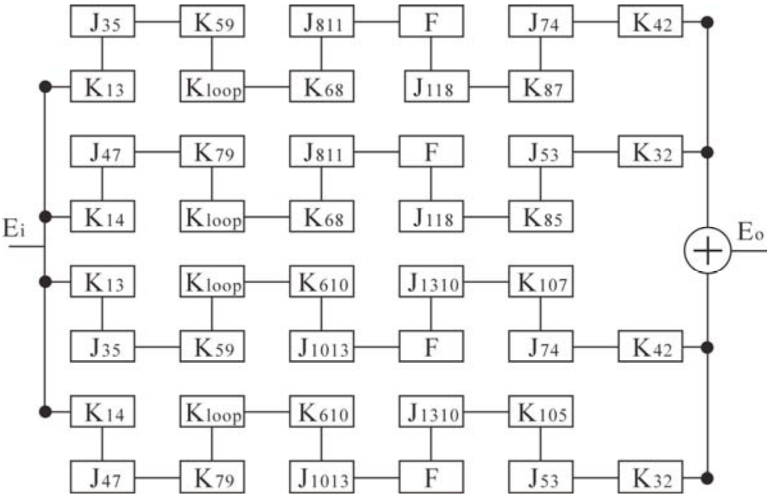

Fig.5. The block diagram of Jones matrix of the fiber optic interferometer

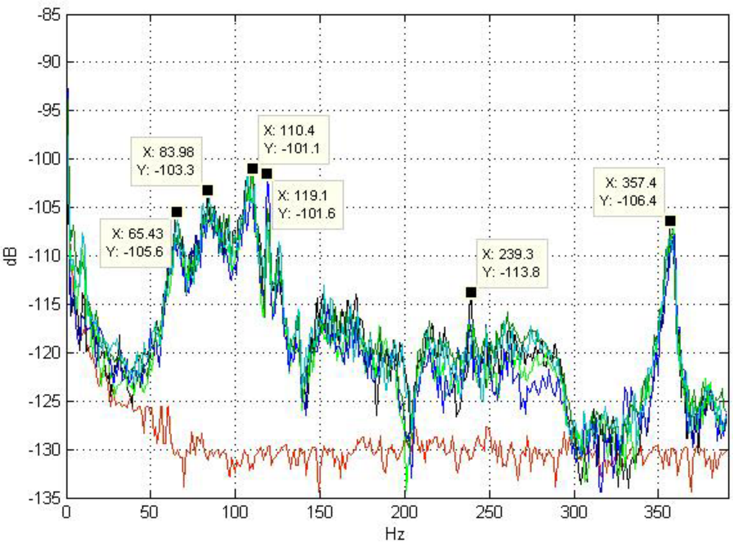

Fig.6. The vibration spectrum of simulated falling stone measured by fiber interferometer